Shell-Structure and Pairing Interaction in Superheavy Nuclei: Rotational Properties of the $Z=104$ Nucleus ^{256}Rf

P. T. Greenlees,[1,*] J. Rubert,[2] J. Piot,[2] B. J. P. Gall,[2] L. L. Andersson,[3] M. Asai,[4] Z. Asfari,[2] D. M. Cox,[3] F. Dechery,[5] O. Dorvaux,[2] T. Grahn,[1] K. Hauschild,[6] G. Henning,[6,7] A. Herzan,[1] R.-D. Herzberg,[3] F. P. Heßberger,[8] U. Jakobsson,[1] P. Jones,[1,†] R. Julin,[1] S. Juutinen,[1] S. Ketelhut,[1] T.-L. Khoo,[7] M. Leino,[1] J. Ljungvall,[6] A. Lopez-Martens,[6] R. Lozeva,[2] P. Nieminen,[1] J. Pakarinen,[9] P. Papadakis,[3] E. Parr,[3] P. Peura,[1] P. Rahkila,[1] S. Rinta-Antila,[1] P. Ruotsalainen,[1] M. Sandzelius,[1] J. Sarén,[1] C. Scholey,[1] D. Seweryniak,[7] J. Sorri,[1] B. Sulignano,[5] Ch. Theisen,[5] J. Uusitalo,[1] and M. Venhart[10]

[1]*Department of Physics, University of Jyväskylä, FIN-40014 Jyväskylä, Finland*
[2]*Institut Pluridisciplinaire Hubert Curien, F-67037 Strasbourg, France*
[3]*Department of Physics, University of Liverpool, Oxford Street, Liverpool, L69 7ZE, United Kingdom*
[4]*Advanced Science Research Center, Japan Atomic Energy Agency, Tokai, Ibaraki 319-1195, Japan*
[5]*CEA, Centre de Saclay, IRFU/Service de Physique Nucléaire, F-91191 Gif-sur-Yvette, France*
[6]*CSNSM, IN2P3-CNRS, F-91405 Orsay Campus, France*
[7]*Argonne National Laboratory, Argonne, Illinois, Illinois 60439, USA*
[8]*GSI, Helmholtzzentrum für Schwerionenforschung GmbH, Planckstr. 1, 64291 Darmstadt, Germany*
[9]*CERN-ISOLDE, Building 26, 1-013, CH-1211 Geneva 23, Switzerland*
[10]*Institute of Physics, Slovak Academy of Sciences, SK-84511 Bratislava, Slovakia*
(Received 4 May 2012; published 3 July 2012)

The rotational band structure of the $Z = 104$ nucleus ^{256}Rf has been observed up to a tentative spin of $20\hbar$ using state-of-the-art γ-ray spectroscopic techniques. This represents the first such measurement in a superheavy nucleus whose stability is entirely derived from the shell-correction energy. The observed rotational properties are compared to those of neighboring nuclei and it is shown that the kinematic and dynamic moments of inertia are sensitive to the underlying single-particle shell structure and the specific location of high-j orbitals. The moments of inertia therefore provide a sensitive test of shell structure and pairing in superheavy nuclei which is essential to ensure the validity of contemporary nuclear models in this mass region. The data obtained show that there is no deformed shell gap at $Z = 104$, which is predicted in a number of current self-consistent mean-field models.

It can be argued that in order to produce a chemical element, the composite nuclear system must survive for more than 10^{-14} seconds. This time is typical for the formation of a compound nucleus or of a molecule such as hydrogen. In turn, a superheavy element can be defined as one in which the macroscopic fission barrier calculated within the liquid drop model would lead to lifetimes lower than this limit. Superheavy elements only exist due to the nuclear shell effect, which gives enhanced stability and results in finite lifetimes. The boundary to superheavy elements occurs at proton number $Z = 104$ [1]. The stability of superheavy elements and the creation of a fission barrier is therefore entirely dependent on shell and pairing effects. Theoretical predictions regarding the structure and stability of superheavy elements can only be rigorously tested if experimental data of high spectroscopic quality is obtained in nuclei with high proton number. It is

well-known that different theoretical approaches predict different locations for the next spherical shell gaps (or magic numbers) beyond the last known doubly-magic nucleus ^{208}Pb with proton number $Z = 82$ and neutron number $N = 126$ (see Refs. [2,3] and references therein for theoretical discussions of shell effects in superheavy nuclei). However, similar differences in shell structure are also predicted for deformed nuclei in the region of $Z = 100$ and $N = 152$. Microscopic-macroscopic [4] approaches predict deformed shell closures at these proton and neutron numbers, but self-consistent approaches based on Skyrme energy density functionals [5] or relativistic mean-field [6] approaches tend to predict deformed gaps at $Z = 96$, 98, 104 and $N = 150$. Comparison with experimental data shows that these discrepancies can be related to the location of the high-j (neutron $j_{15/2}$ and proton $i_{13/2}$) orbitals at sphericity [5,6]. It is important to test these predictions experimentally in order to gain confidence that extrapolations to the heaviest known elements are accurate. Over the past decade or so, exploitation of tagging techniques has allowed "in-beam" studies to be performed, giving new experimental data on rotational bands and associated moments of inertia, alignment properties

and two quasiparticle high-K structures. All of these features are sensitive to the location of the important high-j orbitals mentioned above. These studies have concentrated on the deformed nuclei in the region of ^{254}No with proton number $Z = 102$ and neutron number $N = 152$. A review of experimental progress in this area can be found in Ref. [7]. The first studies of rotational structures in this region prompted a large number of theoretical works which aimed to reproduce the experimental results and to predict the properties of yet unstudied nuclei (see, for example, Refs. [5,6,8]). The work of Bender *et al.* [5] studied the rotational properties of these nuclei in a mean-field approach based on Skyrme-type forces and extended to the rotational properties of ^{256}Rf. To date, it has not been possible to test the predicted properties of $Z = 104$ nuclei due to the fact that they are produced with cross sections at the level of tens of nanobarns, which until recently was beyond the observational limit. Advances in instrumentation have now allowed the first in-beam study of a $Z = 104$ nucleus to be performed, providing a test of the theoretical predictions.

The $Z = 104$ nucleus ^{256}Rf can be produced via the ^{208}Pb(^{50}Ti, $2n$) fusion-evaporation reaction. Previous studies have determined that ^{256}Rf decays by spontaneous fission (branching ratio >98%) with a half-life of 6.7(9) ms [9]. These properties make ^{256}Rf an ideal case to be studied using fission tagging, an extension of the recoil-decay tagging (RDT) technique [10,11]. The experiment was carried out at the Accelerator Laboratory of the Department of Physics, University of Jyväskylä, Finland. A beam of ^{50}Ti^{11+} ions was produced in an ECR ion source using the MIVOC (metallic iIons from volatile compounds) method [12] and accelerated to an energy of 242 MeV by the $K = 130$ MeV cyclotron. The self-supporting ^{208}Pb target had a thickness of 446 μg/cm^2 and was rotated in order to avoid deterioration under irradiation. The total irradiation time was 450 h with an average beam intensity of 29 particle nA. Prompt γ rays were detected using the JUROGAMII array of germanium detectors, consisting of 24 clover- and 15 tapered detectors with Compton suppression shields [13]. The germanium detectors were instrumented with Lyrtech VHS-ADC cards, which allowed direct digitization of the preamplifier signals at a sampling rate of 100 MHz and with 14-bit resolution. The energies of detected γ rays were determined using a moving window deconvolution (MWD) algorithm [14] implemented in the FPGA of the ADC cards. This method allows much higher counting rates to be used compared to conventional analogue electronics, which in turn allows higher beam intensities to be employed (up to 45 pnA in this case). It is estimated that the total number of γ rays detected during the experiment was in excess of 10^{12}. The photopeak efficiency of the array was 5.2% at 1.33 MeV when the add-back method is employed for the clover detectors. Reaction products

recoiling out of the target were separated according to their magnetic rigidity from primary beam and fission products by the gas-filled recoil separator RITU [15]. The pressure of helium filling gas in RITU was 0.6 mbar and a differential pumping system was used to separate the helium filling from the beam line vacuum. The separated reaction products passed through a multi-wire proportional counter (MWPC) and were subsequently implanted into the silicon double-sided strip detectors (DSSDs) of the GREAT focal plane spectrometer system [16]. The MWPC provides a measurement of the energy loss (ΔE) and the time-of-flight (TOF) between the MWPC and DSSDs. In this experiment, two 60×40 mm DSSDs with a strip pitch of 1 mm and thickness 300 μm were placed side-by-side to cover the focal plane image. The amplification of signals from the DSSDs was such that the face containing vertical strips (x face) was set to detect a maximum energy of 2 MeV and that containing horizontal strips (y face) to a maximum energy of approximately 200 MeV. This arrangement was made in order to use the x face for detection of low-energy conversion electrons from the decay of possible isomeric states [17,18] and the y face to detect fission fragments from ^{256}Rf. The energies of events occurring in all detectors were recorded by the triggerless total data readout (TDR) data acquisition system and time stamped using a 100 MHz clock [19]. Subsequent temporal- and spatial-correlations between the various detector groups were performed using the GRAIN data analysis package [20]. Recoiling products were selected on the basis of TOF-ΔE and E-TOF, where E is the energy deposited in the DSSDs by the recoil. Unambiguous identification of fusion-evaporation products of ^{256}Rf was made by demanding that a recoil event was followed by a decay event in the same position with energy greater than $\simeq 20$ MeV within a search time of 100 ms. In the duration of the experiment, a total of 2210 such correlated recoil-fission pairs were found. Assuming a transmission efficiency of 40% and detector coverage of 90%, this corresponds to a production cross section of 17(3) nb. Figure 1 shows the time difference between the recoil and fission event with a logarithmic time scale. The half-life was determined to be 6.9(2) ms, consistent with the previous measurements [9,17,18]. The energy spectrum of correlated fission events found in this manner is shown in the inset to Fig. 1. It should be noted that the observed energy does not correspond to the total energy emitted in the fission process, as the fission fragments can escape the implantation detector. The energy scale is also approximate and based on the observed energies of α decays with the same gain settings.

Prompt γ rays associated with correlated ^{256}Rf recoils were selected by using a two-dimensional polygonal "gate" on a matrix of the MWPC-DSSD TOF versus the time difference between detection of the γ ray and the recoil (essentially two different TOF measurements). The energy spectrum of prompt single γ rays selected in this
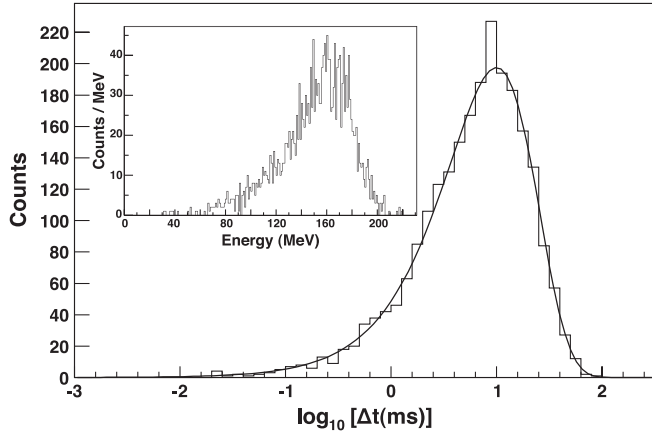
FIG. 1. Time difference between recoil and fission events detected at the same position in the DSSDs within 100 ms. Inset: Energy spectrum of correlated fission events with the same selection criteria.

manner is displayed in Fig. 2. The sensitivity of the method is clearly demonstrated by the fact that in the energy range shown this spectrum contains a total of 745 γ ray events, extracted from a total of more than 10^{12} detected γ rays. A clear, regularly-spaced sequence of eight peaks (labeled with the transition energy) can be seen in the figure along with intense peaks due to Rf and Pb x rays. Such a sequence of regularly spaced transitions is characteristic of rotational bands established in other nuclei in the region, for example, in ^{254}No. In fact, the similarity between the transition energies in ^{256}Rf and ^{254}No is remarkable. Thus, the sequence of transitions with energies 161, 218, 272, 323, 371, 417, 459, and 499 keV are assigned to form a rotational band in ^{256}Rf, showing that ^{256}Rf is a deformed nucleus.

A fit to the rotational band based on the experimental kinematic moment of inertia $\mathcal{J}^{(1)} = \hbar^2(2I-1)/E_\gamma(I)$ can also be used to assign spin values to the observed states.
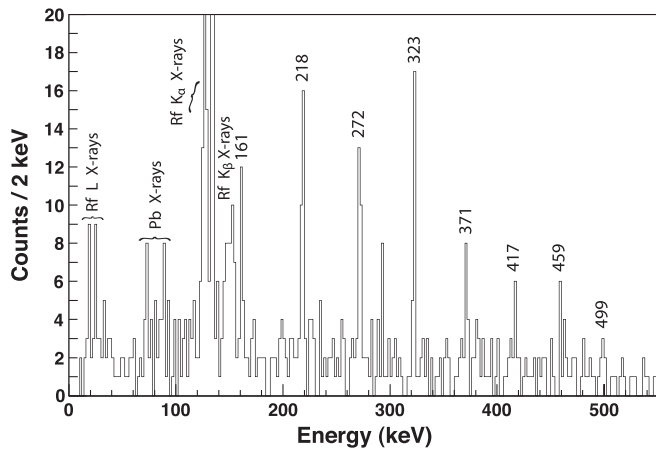

FIG. 2. Energy spectrum of prompt singles γ rays associated with fission-tagged ^{256}Rf recoils.

Table I shows the transition energies, spin assignments and relative intensities of the transitions corrected for efficiency and internal conversion. It is also possible to parameterize the rotational band in terms of the kinematic ($\mathcal{J}^{(1)}$) and dynamic ($\mathcal{J}^{(2)}$) moments of inertia according to the formalism of Harris [21], whereby

$$\mathcal{J}^{(1)} = \mathcal{J}_0 + \mathcal{J}_1 \omega^2, \tag{1}$$

$$\mathcal{J}^{(2)} = \mathcal{J}_0 + 3\mathcal{J}_1 \omega^2, \tag{2}$$

where ω is the rotational frequency ($E_\gamma/2$). After fitting the Harris parameters $\mathcal{J}_0$ and $\mathcal{J}_1$ it is then possible to extrapolate and determine the energies of the unobserved 4^+ to 2^+ and 2^+ to 0^+ transitions using the formula

$$I = \mathcal{J}_0 \omega + \mathcal{J}_1 \omega^3 + 1/2, \tag{3}$$

where I is the initial spin for the transition. The Harris parameters fitted for the rotational band of ^{256}Rf are $\mathcal{J}_0 = 66.7\hbar^2\,\mathrm{MeV}^{-1}$ and $\mathcal{J}_1 = 175.5\hbar^2\,\mathrm{MeV}^{-3}$. The two lowest-lying transitions cannot be observed due to the dominance of internal conversion. The deduced energies of the 4^+ to 2^+ and 2^+ to 0^+ transitions are also shown in Table I.

It is well-known that the moments of inertia are sensitive to nuclear properties such as the pairing strength and to the specific orbitals active at the Fermi surface. A systematic analysis of the moments of inertia of a number of nuclei can therefore provide invaluable information on such properties in these heavy nuclei. The kinematic moment of inertia as a function of rotational frequency for the ground-state rotational band of ^{256}Rf is shown in the upper panel Fig. 3 and compared to that of ^{250}Fm, ^{252}No and ^{254}No. The lines drawn are from Harris fits to the low-spin part of the data and plotted according to Eq. (1). The moment of inertia of ^{256}Rf shows very similar behavior as a function of rotational frequency as the $N = 152$ isotone ^{254}No, though the absolute value is slightly lower over

TABLE I. Calculated energies of the 4^+ to 2^+ and 2^+ to 0^+ transitions, measured transition energies and tentative transition assignments for the rotational band of ^{256}Rf. The last column shows the relative intensities of the transitions corrected for efficiency and internal conversion.

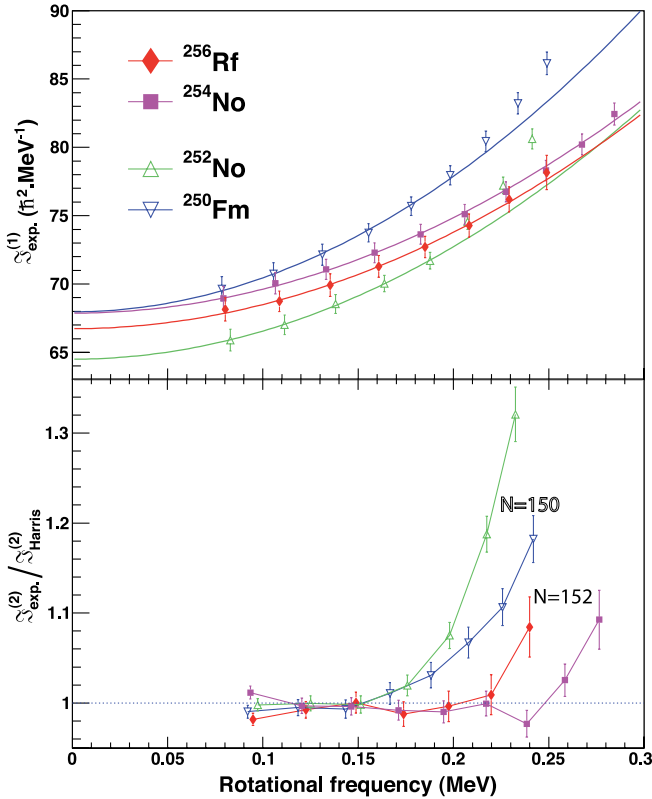| E_γ (keV)	Transition assignment	Relative intensity (%)
44 ± 1	$(2^+ \to 0^+)$	
104 ± 1	$(4^+ \to 2^+)$	
161 ± 1	$(6^+ \to 4^+)$	100 ± 30
218 ± 1	$(8^+ \to 6^+)$	80 ± 20
272 ± 1	$(10^+ \to 8^+)$	53 ± 12
323 ± 1	$(12^+ \to 10^+)$	49 ± 11
371 ± 1	$(14^+ \to 12^+)$	22 ± 8
417 ± 2	$(16^+ \to 14^+)$	20 ± 7
459 ± 2	$(18^+ \to 16^+)$	18 ± 7
499 ± 2	$(20^+ \to 18^+)$	16 ± 7

FIG. 3 (color online).   Upper panel: Kinematic moment of inertia as a function of rotational frequency for $N = 150$ and $N = 152$ isotones. The lines are drawn according to fits of the Harris parameters and using Eq. (1). Lower panel: Dynamic moment of inertia of the $N = 150$ and $N = 152$ isotones, normalized to that calculated using the fitted Harris parameters and Eq. (2).

the full frequency range. As has been noted previously, the rotational properties of the $N = 150$ isotones are somewhat different, showing much faster alignment than the $N = 152$ nuclei (for a discussion see Refs. [5,22]). It is interesting to question the differences in absolute value of the moments of inertia in these nuclei. It can be seen that while the $N = 150$ isotones show similar alignment behavior, ^{250}Fm has a larger moment of inertia than ^{252}No. At low frequency, ^{254}No has a similar moment of inertia to ^{250}Fm, but slightly higher than that of ^{256}Rf. It is possible that these changes in the moment of inertia are due to differences in deformation, or, as discussed by several authors, due to the effect of shell gaps on the pairing correlations [4,6]. At a deformed shell gap, the pairing correlations are weakened, which in turn leads to a larger moment of inertia. This seems to be borne out by the behavior of the moments of inertia plotted in Fig. 3. The nucleus ^{252}No has the lowest moment of inertia, which having 102 protons and 150 neutrons has the Fermi surface just above the $Z = 100$ and just below the $N = 152$ deformed shell gaps. When two protons are removed to get ^{250}Fm, the moment of inertia increases, which may be a

reflection of the reduced pairing correlations due to the $Z = 100$ shell gap. A similar argument goes for ^{254}No, in which the moment of inertia is larger when two neutrons are added compared to ^{252}No. Again, this is evidence of the influence of the $N = 152$ shell gap. Table II shows the experimental 2^+ energies deduced from extrapolation of the rotational bands, the fitted $\mathcal{J}_0$ Harris parameter and the calculated quadrupole deformation parameter β_2 and 2^+ energies from the work of Sobiczewski *et al.* [4]. It can be seen that the calculated β_2 deformation parameters for all nuclei are approximately equal, lending support to the argument that the subtle differences in moment of inertia are due to pairing effects. Following these arguments, one would expect that ^{252}Fm with $Z = 100$ and $N = 152$ should have the highest moment of inertia and lowest 2^+ energy, but unfortunately the experimental data is not yet available. It might also be expected that if there is a significant shell gap at $Z = 104$, that the moment of inertia of ^{256}Rf would be larger than that of the isotone ^{254}No. As can be seen from Fig. 3 and Table II, this is not the case. In fact the moment of inertia is slightly lower, which may be indicative of the diminishing influence of the $Z = 100$ shell gap. On the basis of this analysis, it can thus be suggested that there is no significant deformed shell gap at $Z = 104$.

The lower panel of Fig. 3 shows the experimental dynamic moment of inertia ($\mathcal{J}^{(2)} = 4\hbar^2/[E_\gamma(I) - E_\gamma(I-2)]$) as a function of rotational frequency for the $N = 150$ and 152 isotones, normalized to the smoothly-behaving $\mathcal{J}^{(2)}$ from the Harris fit. The behavior at low rotational frequency is similar for all nuclei, but a divergence from the smooth behavior appears above frequencies of around 0.15 MeV in the $N = 150$ isotones and above 0.2 MeV in the $N = 152$ nuclei, indicating an alignment effect. It is interesting to note that the alignment occurs simultaneously in the $N = 150$ isotones, but appears later in the $N = 152$ isotones and is delayed in ^{254}No relative to ^{256}Rf. It has been shown that in this region of nuclei there is competition between neutron $j_{15/2}$ and proton $i_{13/2}$ alignment effects [6,23]. These effects are sensitive to the relative positions of the relevant orbitals to the Fermi surface. In $N = 150$ isotones, the Fermi surface is just below the neutron $j_{15/2}$ [734]9/2$^-$ orbital, which is filled in $N = 152$ nuclei. Given that ^{254}No and ^{256}Rf are

TABLE II.   Experimental 2^+ energies deduced from an extrapolation of the rotational bands, $\mathcal{J}_0$ values and theoretical β_2 and $E(2^+)$ values taken from Sobiczewski *et al.* [4]).

Nucleus	$E(2^+)$ Expt.(keV)	$\mathcal{J}_0$	β_2 [4]	$E(2^+)$ [4] (keV)
^{250}Fm	44.0	68.1	0.248	43.9
^{252}Fm	$\cdots$	$\cdots$	0.250	42.0
^{252}No	46.4	64.4	0.249	44.5
^{254}No	44.1	68.0	0.252	41.6
^{256}Rf	44.8	66.7	0.249	43.4

isotones, it could be speculated that the difference is due to the shift of the proton Fermi surface in moving from ^{254}No to ^{256}Rf. In ^{256}Rf the proton Fermi surface is closer to the $i_{13/2}$ orbital $[624]9/2^+$. Further detailed theoretical investigation based on a model which correctly predicts the underlying single-particle levels would be required to explain these subtle differences in detail.

In summary, the rotational structure of the superheavy $Z = 104$ nucleus ^{256}Rf has been studied for the first time using novel γ-ray spectroscopic techniques. Systematic analysis of the moment of inertia of several nuclei shows evidence for the effect of weakened pairing correlations due to the presence of deformed shell gaps. The data also suggest that there is no significant shell gap at $Z = 104$. Differences in the alignment properties $N = 150$ isotones and of ^{254}No and ^{256}Rf are observed and suggested to be related to the relative proximity of the neutron $j_{15/2}$ and proton $i_{13/2}$ orbitals to the Fermi surface.

---

*paul.greenlees@jyu.fi

[†]Present Address: Department of Nuclear Physics, iThemba Labs, Somerset West 7219, South Africa.

[1] M. Schädel, Angew. Chem., Int. Ed. **45**, 368 (2006).
[2] M. Bender, K. Rutz, P. G. Reinhard, J. A. Maruhn, and W. Greiner, Phys. Rev. C **60**, 034304 (1999).
[3] A. V. Afanasjev, H. Abusara, E. Litvinova, and P. Ring, J. Phys. Conf. Ser. **312**, 092004 (2011).
[4] A. Sobiczewski, I. Muntian, and Z. Patyk, Phys. Rev. C **63**, 034306 (2001).
[5] M. Bender, P. Bonche, T. Duguet, and P.-H. Heenen, Nucl. Phys. **A723**, 354 (2003).
[6] A. V. Afanasjev, T. L. Khoo, S. Frauendorf, G. A. Lalazissis, and I. Ahmad, Phys. Rev. C **67**, 024309 (2003).
[7] R.-D. Herzberg and P. T. Greenlees, Prog. Part. Nucl. Phys. **61**, 674 (2008).
[8] T. Duguet, P. Bonche, and P.-H. Heenen, Nucl. Phys. **A679**, 427 (2001).
[9] B. Sulignano, Ph.D. thesis, Johannes Gutenberg Universität Mainz, 2007.
[10] K.-H. Schmidt, R. S. Simon, J.-G. Keller, F. P. Hessberger, G. Münzenberg, and B. Quint, H.-G. Clerc, W. Schwab, U. Gollerthan, and C.-C. Sahm Phys. Lett. B **168**, 39 (1986).
[11] E. Paul et al., Phys. Rev. C **51**, 78 (1995).
[12] J. Rubert, J. Piot, Z. Asfari, B. JP. Gall, J. Ärje, O. Dorvaux, P. T. Greenlees, H. Koivisto, A. Ouadi, R. Seppälä, Nucl. Instrum. Methods Phys. Res., Sect. B **276**, 33 (2012).
[13] P. Nolan, F. Beck, and D. Fossan, Annu. Rev. Nucl. Part. Sci. **44**, 561 (1994).
[14] A. Georgiev and W. Gast, IEEE Trans. Nucl. Sci. **40**, 770 (1993).
[15] M. Leino et al., Nucl. Instrum. Methods Phys. Res., Sect. B **99**, 653 (1995).
[16] R. Page et al., Nucl. Instrum. Methods Phys. Res., Sect. B **204**, 634 (2003).
[17] H. Jeppesen et al., Phys. Rev. C **79**, 031303(R) (2009).
[18] A. Robinson et al., Phys. Rev. C **83**, 064311 (2011).
[19] I. Lazarus et al., IEEE Trans. Nucl. Sci. **48**, 567 (2001).
[20] P. Rahkila, Nucl. Instrum. Methods Phys. Res., Sect. A **595**, 637 (2008).
[21] S. Harris, Phys. Rev. **138**, B509 (1965).
[22] R.-D. Herzberg et al., Phys. Rev. C **65**, 014303 (2001).
[23] F. Al-Khudair, G.-L. Long, and Y. Sun, Phys. Rev. C **79**, 034320 (2009).